Journal of Applied Polymer Science

Solution processed low-k dielectric core-shell nanoparticles for additive manufacturing of microwave devices

Shamus O'Keefe, Yilin Li, Christine K. Luscombe
Materials Science and Engineering Department, University of Washington, Seattle Washington 98195-2120
Correspondence to: C.K. Luscombe (E-mail: luscombe@uw.edu)

ABSTRACT: This study introduces a new core-shell structured polytetrafluoroethylene (PTFE)/polyimide (PI) nanoparticle for additive manufacturing of microwave substrates. Materials were synthesized using a solution processed method through the electrostatic interaction between PTFE with negative potential and poly(amic) acid salt (PAAS, a PI precursor) with positive potential followed by the thermal imidization of PAAS. Microscopic studies by transmission electron microscopy, scanning electron microscopy, and atomic force microscopy confirmed the formation of core-shell nanoparticles, a porous material network, and a reduction of surface roughness upon imidization. In addition to excellent high temperature stability (<0.4% weight loss at 500 °C), the synthesized materials showed improved particle-to-particle adhesion and particle-to-substrate adhesion compared to PTFE alone, and good dielectric properties measured at 7.2 GHz utilizing a cavity perturbation technique. The materials consisting of 5% to 35% of PI exhibited low relative permittivity (ε') of 2.14 to 2.38 and loss tangent (tan δ) of 0.001 to 0.0018, which make them well suited for use in additive manufacturing. © 2017 Wiley Periodicals, Inc. J. Appl. Polym. Sci. **2017**, *134*, 45335.

KEYWORDS: applications; composites; dielectric properties; manufacturing; nanocrystals; nanoparticles; nanowires

Received 2 March 2017; accepted 21 May 2017
DOI: 10.1002/app.45335

INTRODUCTION

Additive manufacturing continues to garner attention from manufacturing companies in recent years due to reported advantages of low cost, high quality, and reduced waste over traditional subtractive manufacturing.[1–3] Though approaches to replacing traditional subtractive processes with additive ones have been broadly studied by many researchers,[4–8] the most basic substrates, widely made from FR-4 (flame retardant), continue to be made in bulk, offline, and later cut to size. Similarly, substrates for microwave devices made from polytetrafluoroethylene (PTFE) are laminate materials made in large batch operations. PTFE, by itself, has never been reported to be used as feedstock in an additive process, largely due to its physical properties, namely its high melt viscosity and low solubility in all common solvents.[9,10] To realize an additive process for microwave substrate manufacturing, fundamental materials science obstacles must be overcome.

A viable solution is to create a composite material that incorporates additional material(s) capable of surmounting the inherent disadvantage(s) sometimes presented by PTFE. One approach is to use homogeneous multiphase PTFE containing composites. Xiang *et al.* reported PTFE/Bi-based composites for microwave use.[11] Thomas *et al.* reported on PTFE/$ZnAl_2O_4$-TiO_2 and PTFE/$Sm_2Si_2O_7$.[12,13] More recently, Jin *et al.* reported on PTFE/$SrTiO_3$ and PTFE/BNT composites for use in RF antennas.[14,15] While these powder processing techniques have proved useful, it has proven difficult via traditional bulk mixing techniques to achieve sample homogeniety due to the poor adhesion of PTFE particles to the binder matrix, which ultimately manifests a low degree of dispersion.[16] Another approach is to utilize a core-shell structure, in which individual PTFE particles are encapsulated by other material(s) to form nanoscale particles. Antonioli *et al.* reported on PTFE/PMMA core-shell nanoparticles for self-assembled opals.[17] This approach will make homogenous dispersion in the bulk automatic.[18] Furthermore, the ratio of components is simply controlled via shell thickness.

Developing a core-shell nanoparticle specifically for the additive manufacturing of microwave device substrates requires a focus on dielectric properties. Because PTFE has a ε' of 2.1 and tan δ less than 0.0001,[19] the shell material(s) used for PTFE based core-shell nanoparticles should have dielectric properties close to PTFE. We previously reported on the viability of aerosol deposition PTFE/polyacrylate (PA) core-shell nanoparticles for microwave substrate manufacturing, achieving a ε' of 2.33 and tan δ of 0.00021.[20] However, the PA shell lacks high temperature stability making PTFE/PA core-shell nanoparticles unqualified for commercial use. Polyimide (PI) has been reported to have ε' as low as 2.5 and tan δ as low as 0.0015.[21] The use of

Table I. Mass of PTFE and PAAS Used for Synthesis of PTFE/PI Core-Shell Nanoparticles

Sample (wt %)	PTFE (g)	PAAS (g)
95% PTFE/5% PI	0.53	0.028
90% PTFE/10% PI	0.53	0.053
75% PTFE/25% PI	0.53	0.18
65% PTFE/35% PI	0.53	0.28

PI in a core-shell nanoparticle would provide excellent high temperature stability of nanoparticle with minimal influence on the particle's dielectric properties.[22] Therefore, replacing the PA with PI would render a nanoparticle suitable for commercial use. In addition, PIs favorable adhesion characteristics, evidenced by its past wide use as a high-performance adhesive,[23] could provide useful in noncontact additive manufacturing techniques where particle-particle and particle-substrate adhesion is critical.

Herein we discuss a new type of core-shell nanoparticle with PTFE core and PI shell with outstanding thermal stability and excellent microwave dielectric properties that can potentially realize an additive process for microwave substrate manufacturing. A series of PTFE/PI nanoparticles were prepared with different PI shell thickness through the electrostatic interaction between PTFE nanoparticles and poly(amic) acid salt (PAAS, a PI precursor) and was further characterized by Fourier transform infrared spectroscopy (FTIR) for composition analysis, transmission electron microscope (TEM) for nanoparticle shape study, and scanning electron microscope (SEM) and atomic force microscopy (AFM) for surface morphology study. In addition to excellent thermal stability from differential scanning calorimetry (DSC) and thermal gravimetric analysis (TGA), results from adhesion testing and dielectric measurements on the aerosol deposited samples were in the range deemed acceptable for microwave device use.

EXPERIMENTAL

Materials

Monomers 4,4′-(hexafluoroisopropylidene) diphthalic anhydride, and 4,4′-oxydianiline were purchased from TCI Chemicals; PTFE nanoparticles (60% aqueous dispersion), *N*-methyl-2-pyrrolidone (NMP), and triethylamine were purchased from Sigma-Aldrich. All materials were used as received.

Synthesis of PAAS

PAAS was synthesized using a two-step procedure, involving the synthesis of PAA, followed by conversion to PAAS.[24] Briefly, 4,4′-oxydianiline (0.17 g, 0.82 mmol) in NMP (5 wt %, 4.9 mL) was stirred at 300 rpm for 30 min under a N_2 atmosphere in a 50 mL round-bottom flask, followed by the addition of 4,4′-(hexafluoroisopropylidene) diphthalic anhydride (0.37 g, 0.82 mmol) in NMP solution (5 wt %, 4.9 mL) with continued stirring for 8 h. A 10% molar excess of triethylamine (0.2 mL) was then added and stirred for 2 h. The solution was added dropwise into acetone (500 mL) to render a solid white precipitate of PAAS.

Synthesis of PTFE/PI Core-Shell Nanoparticles

A series of PTFE/PI core-shell nanoparticles were prepared with different PI shell thickness, controlled by the mass of PI added, as depicted in Table I. Figure 1 illustrates the synthetic method.

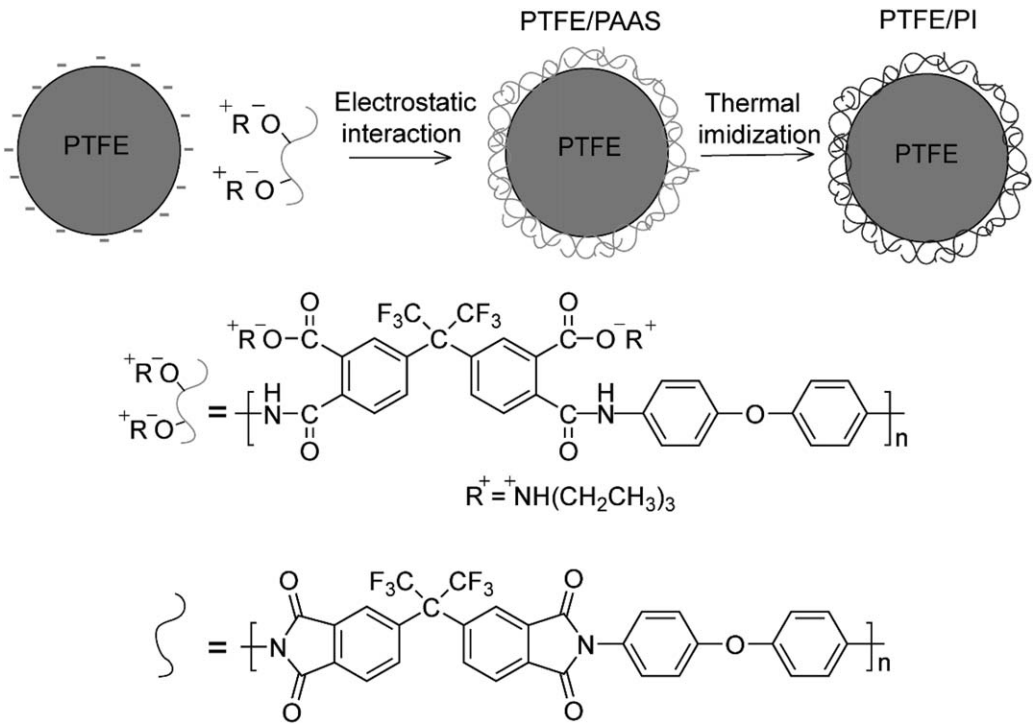

Figure 1. Schematic illustration of self-assembly of polytetrafluoroethylene (PTFE) nanoparticles and poly(amic) acid salt (PAAS) via electronic interaction.

An example is given here to show the synthetic protocol of nanoparticles containing 95 wt % PTFE and 5 wt % PI. A PTFE aqueous dispersion (0.88 g containing 0.53 g PTFE) was first added to deionized water (100 mL) in a 250 mL round-bottom flask with stirring at 250 rpm for 10 min. The clear solution was heated to 40 °C and the PAAS (0.028 g) was added and allowed to completely dissolve over a period of 45 min. Stirring at 100 rpm for 8 h yielded a solid suspension. 50 mL quantities of the mixture were added to a PTFE lined autoclave and heated at 150 °C for 12 h to fully imidize the PAAS shell; a 10 mL aliquot was reserved for TEM grid preparation(s). The nanoparticles were centrifuged, redispersed in deionized water, and centrifuged a final time.

Sample Preparation and Characterization

Zeta potential of the PTFE aqueous dispersion was measured using a Zetasizer (NanoZS, Malvern Instruments). Samples for DSC (Q200, TA Instruments) and TGA (Q50, TA Instruments) were prepared by drying the centrifuged nanoparticles under vacuum (25 mmHg) at 60 °C for 24 h. Both were measured under an N_2 atmosphere at a heating rate of 10 °C/min. Samples for FTIR (Bruker Vertex 70 w/ATR), SEM (Sirion XL30, FEI), and AFM (Bruker Dimension Icon-PT) were prepared by redispersing the centrifuged nanoparticles in deionized water to make a 5 wt % solution, followed by drop casting onto a sodium borosilicate glass slide and drying under vacuum (25 mmHg) at 60 °C for 24 h. Samples for SEM were Au sputtered prior to surface scanning. Samples for TEM (Technai G2 F20, FEI) were prepared by dispersing two drops of a 1 wt % solution onto a carbon coated copper TEM grid (400 mesh) followed by exposure to ruthenium vapors for 1 h. Samples for adhesion testing and dielectric spectroscopy with approximate 2 μm thick were prepared by aerosol spraying a 5 wt % solution onto a sodium borosilicate glass slide heated to 70 °C. Adhesion characterization was performed using 3 M 610 tape in accordance with ASTM F2252. Dielectric spectroscopy was performed at 7.2 GHz utilizing a cavity perturbation technique. The significance for choosing 7.2 GHz in dielectric spectroscopy is because (1) it falls in range of microwave frequencies, specifically the X-band 7 to 12 GHz, and (2) the cavity perturbation technique used herein utilizes a waveguide as the cavity resonator and at 7.2 GHz there exists a particularly sharp and well-defined resonant peak. Such a sharp, well-defined peak is ideal for performing cavity perturbation measurements. For the cavity perturbation measurements, a typical WR-90 X-band waveguide was used as the cavity with a small opening machined in the center position of the top of the waveguide. This position coincides with the maximum electric field of the TE_{10N} modes (N = odd). The waveguide was connected to a Hewlett Packard HP8510C Vector Network Analyzer. To measure the thin polymer film properties, first a bare substrate is inserted into the cavity and the f_c and Q_c are recorded. Then once the substrate has been coated with the polymer film, it is inserted into the cavity and again, the f_s and Q_s are recorded.

Both ε' and ε'' can be calculated from the changes in the resonant frequencies (i.e., f_c and f_s) and quality factors (i.e., Q_c and Q_s) that result when the sample is inserted in the cavity:[25,26]

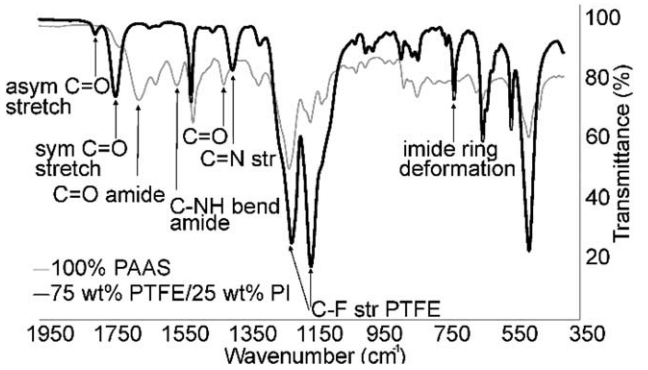

Figure 2. Fourier transform infrared (FTIR) analysis of poly(amic) acid salt (PAAS) and polytetrafluoroethylene (PTFE)/polyimide (PI) core-shell nanoparticles.

$$\varepsilon' = \frac{V_c(f_c - f_s)}{2V_s f_s} + 1 \quad (1)$$

$$\varepsilon'' = \frac{V_c}{4V_s}\left(\frac{1}{Q_s} - \frac{1}{Q'_c}\right) \quad (2)$$

$$Q'_c = Q_c\left[1 + (\varepsilon' - 1)\frac{V_s}{V_c}\right] \quad (3)$$

$$\tan\delta = \frac{\varepsilon''}{\varepsilon'} \quad (4)$$

RESULTS AND DISCUSSION

Material Synthesis

The preparation of a PTFE/PI core-shell nanoparticle via self-assembly of PTFE nanoparticle and PAAS followed by thermal imidization is shown in Figure 1. The zeta potential of PTFE aqueous dispersion was −37.2 mV, suggesting that the PTFE nanoparticles were highly negatively charged. In contrast, the PAAS is known to be slightly positively charged due to the presence of the quaternary ammonium groups.[27] The negative and positive potential create coulombic attraction between the PTFE and PAAS, enabling the reaction through electrostatic interaction. After careful addition of PAAS to the PTFE aqueous dispersion, particle coagulation was observed, indicating that the PAAS had self-assembled onto the PTFE nanoparticles through electrostatic interaction. This was further confirmed after thermal imidization and centrifugation, when the clear supernatant was poured into excess acetone, revealing no precipitation, thus indicating complete assembly of PAAS onto PTFE. Our later FTIR analysis (discussed in next section, Figure 2) proved the successful incorporation of PI with PTFE to form PTFE/PI composites while further microscopic study using TEM (discussed later, Figure 3) proved that the PTFE/PI composite do in fact possess a core-shell structure. A facile synthesis such as this is favorable for additive manufacturing for several reasons: (1) an aqueous medium with little or no remnants of reactant chemicals is typically nontoxic and requires only modest heat to drive off moisture following noncontact deposition such as aerosol or inkjet printing; (2) the synthesis reaction is not complex and requires no special equipment other than modest heat; and (3) the synthesis scales easily to produce large quantities suitable for commercial use.

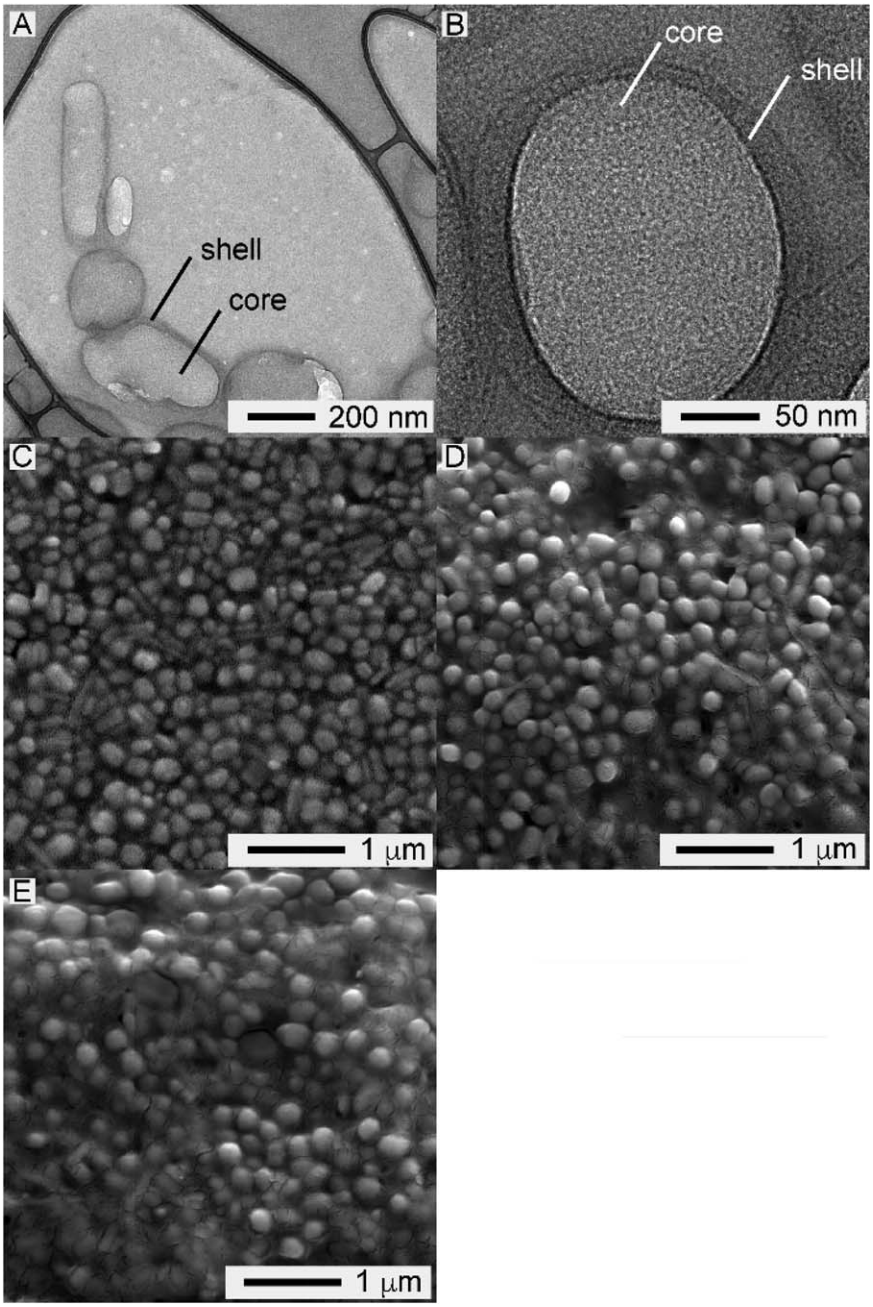

Figure 3. Transmission electron microscope (TEM) images of (A) 90% polytetrafluoroethylene (PTFE)/10% polyimide (PI) core-shell nanoparticles and (B) a 75% PTFE/25% PI core-shell nanoparticle; SEM images of (C) as-received PTFE particle, (D) 90% PTFE/10% poly(amic) acid salt (PAAS) core-shell nanoparticles, and (E) 90% PTFE/10% PI core-shell nanoparticles.

FTIR Analysis

To prove that the PI had been successfully incorporated with PTFE, FTIR analysis was conducted on the synthesized composite, which is shown in Figure 2. A 100% PAAS spectrum is shown as a baseline prior to thermal imidization. The spectrum clearly shows the characteristic absorption peaks of PAAS at 1656, 1546, and 1404 cm^{-1}, attributed to the C═O of the amide, the amide C—NH bend, and C═O of –COOH, respectively. The 75% PTFE/25% PI spectrum shows the new characteristic absorption peaks of PI. The presence of peaks at 1786, 1720, 1375, and 725 cm^{-1} can be attributed to the asymmetric C═O stretch, symmetric C═O stretch, C—N stretch, and imide ring deformation, respectively. The 75% PTFE/25% PI spectrum also clearly shows the characteristic absorption peaks of PTFE at 1202 and 1145 cm^{-1}, attributed to the C—F stretch. FTIR analysis shows that the imide ring formation occurred to completion following thermal imidization as revealed by the complete disappearance of the C═O amide peak (1656 cm^{-1}) and C—NH bend peak (1546 cm^{-1}), and the appearance of the imide ring peak (725 cm^{-1}).

Microscopy Study

Compared to the FTIR analysis which only provides information on the incorporation of PI to PTFE after synthesis, images of the composites obtained from TEM and SEM provides critical information, suggesting that the PTFE/PI composites have a core-shell structure. The shape and morphology of the synthesized materials were characterized by TEM and SEM, respectively and can be seen in Figure 3. TEM images shown in Figure 3(A) (90% PTFE/10% PI) and (B) (75% PTFE/25% PI) clearly show that the PTFE nanoparticles become encapsulated within the PI shells. A thicker PI shell in 75% PTFE/25% PI nanoparticle sample (22 nm compared to 9 nm for the 90% PTFE/10% PI nanoparticle sample) is consistent with the material synthesis protocols that the thickness of the PI shell is controlled by the amount of PI added into the reaction. These TEM images also show that there is no void space between the core(s) and shell(s), indicating a strong interaction between PTFE and PI. A strong coupling between the core and shell is important when considering the bulk dispersion of PTFE amongst PI; when the coupling is strong and no separation of the shell from the core occurs, a homogeneous dispersion can be formed provided the shell thickness from particle to particle is uniform. Poor dispersion leads to nonuniform properties, which is undesirable for microwave substrates.

Morphology of a drop cast film, in the form of SEM and AFM images, of PTFE nanoparticles, 90% PTFE/10% PAAS core-shell nanoparticles, and 90% PTFE/10% PI core-shell nanoparticles can be seen in Figures 3(C–E) and 4(A–C). PTFE nanoparticles are approximately 200 nm as seen in Figure 3(C). Figure 3(D,E) clearly shows individual PTFE particles residing in the PAAS and PI matrix, respectively, after the introduction of PAAS followed by thermal imidization on a hot plate at 150 °C for 15 min. Upon careful examination, one can see that the PAAS shells coalesce and form a more continuous matrix once imidized to PI while there remains appreciable porosity between individual particles within the film. Indeed, some porosity and free volume between polymer chains is desirable when it is homogeneous throughout the solid due to its effective lowering of the ε' because of the low ε' of air ($\varepsilon' = 1$).[28] The more porous, the more surface area the nanoparticles have; however, porosity encountered on external boundaries (i.e., surfaces) will increase the chance of water absorption,[29] which is highly undesirable because water absorption contributes to an increase in the ε' because of the high ε' of water ($\varepsilon' = 80$).[30] The formation of a continuous PI matrix after thermal imidization of PAAS reduces the porosity on external boundaries and thus can help to decrease the water absorption. This is further supported by the surface roughness measurements by AFM. A reduction of the surface roughness is clearly observed in the AFM image of 90% PTFE/10% PI [Figure 4(c)] compare to PTFE, 90% PTFE/10% PAAS [Figure 4(b)] and PTFE [Figure 4(c)]. The root mean square values obtained from surface roughness measurements for PTFE, 90% PTFE/10% PAAS, and 90% PTFE/10% PI are 58, 59, and 49 nm, respectively. The combination of remnant porosity within the film and decreased surface roughness provided a low ε' film upon imidization (discussed later in Figure 6).

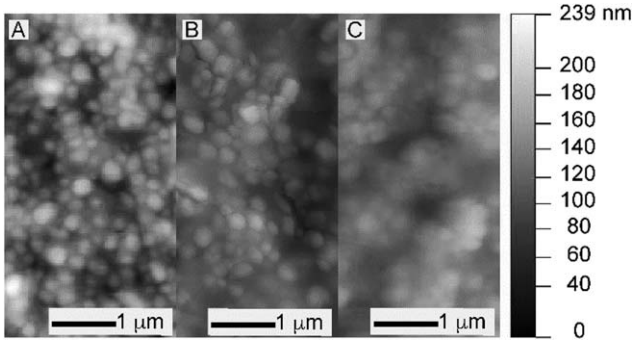

Figure 4. Atomic force microscopy (AFM) images of (A) as-received polytetrafluoroethylene (PTFE) particles, (B) 90% PTFE/10% poly(amic) acid salt (PAAS) core-shell nanoparticles, and (C) 90% PTFE/10% polyimide (PI) core-shell nanoparticles.

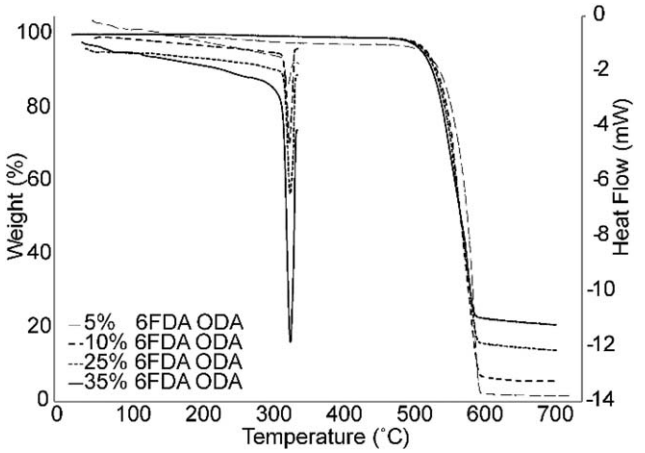

Figure 5. Differential scanning calorimetry (DSC) curves and thermal gravimetric analysis (TGA) curves for different wt % polytetrafluoroethylene (PTFE)/polyimide (PI) core-shell nanoparticles.

Properties of Nanoparticles

After characterizing the PTFE/PI core-shell nanoparticle in terms of PI incorporation, nanoparticle shape, and surface morphology, the PTFE/PI core-shell nanoparticles were characterized for their thermal, adhesion, and dielectric properties, as they pertain to additive manufacturing.

The thermal properties of PTFE/PI core-shell nanoparticles were examined using DSC and TGA, as seen in Figure 5. The DSC curves for all wt % clearly show the characteristic PTFE endotherm near 330 °C, as reported elsewhere.[31] The magnitude of the endotherm increases with increasing wt % PI (or decreasing wt % PTFE) indicating that the endothermic enthalpy of PI is higher than PTFE. The thermal stability of all wt % can also be seen in Figure 5. The decomposition temperature (defined as 5% of total weight loss) decreases slightly 528 to 524 °C as the wt % PI increases compared to 100% PTFE (535 °C). This slight reduction in thermal stability of the PTFE/PI core-shell nanoparticles can be attributed to the markedly lower thermal

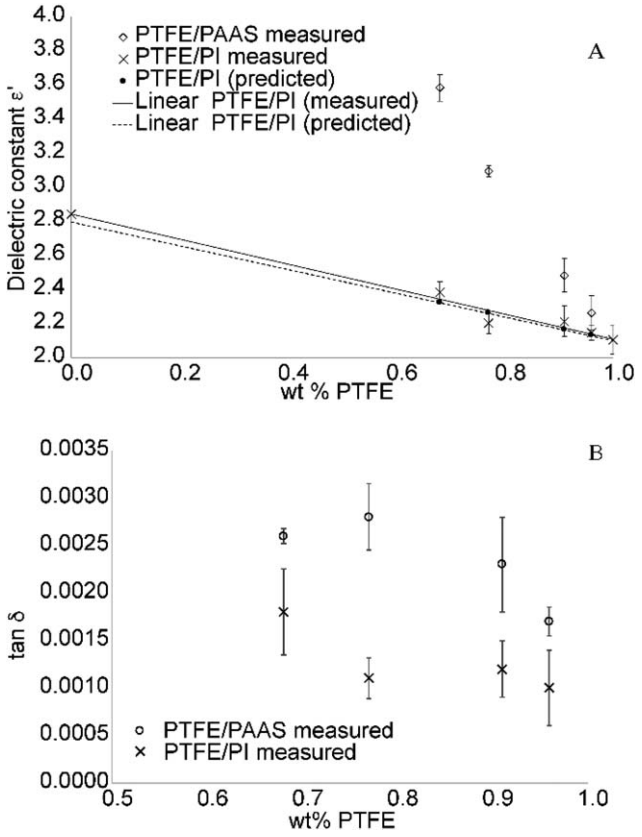

Figure 6. Measured and predicted (A) ε′ and (B) tan δ for various wt % polytetrafluoroethylene (PTFE)/poly(amic) acid salt (PAAS) and PTFE/polyimide (PI) core-shell nanoparticles. Note: The ε′ for 100% PTFE was measured using a commercially available PTFE film 5 μm in thickness.

conductivity of PI (0.00524 W/m K) versus that of PTFE (0.25 W/m K).[32] It is believed that the lower thermal conductivity of PI impedes the release of heat from the external surfaces, trapping interior heat which results in an earlier decomposition temperature. Even so, the thermal properties of PTFE/PI core-shell nanoparticles are improved compared to our previously reported PTFE/PA core-shell nanoparticles.[20]

The adhesion properties of aerosol sprayed samples were characterized using a tape test in accordance with ASTM F2252–03 Standard Practice for Evaluating Ink or Coating Adhesion to Flexible Packaging Materials Using Tape.[33] In this method, the external force is applied by the thumb or forefinger (no specified force value is provided) along the tape to make sure it is fully adhered, without any bubbles in surface. Good adhesion is particularly important for noncontact deposition processes to ensure longevity and durability of the material once deposited onto the build substrate. Five samples were prepared for each wt %, including 100% PTFE. Results are reported in Table II. 100% PTFE failed all five trials, while each wt % PI sample passed a minimum of three of five trials. The ability to provide substrate adhesion and particle to particle adhesion is due to the presence of the PI shell. PI has long been utilized across multiple industries as a high-performance structural adhesive,[34] thus it is expected that at even small wt % PI content, significant improvement in adhesion would be observed.

To investigate the dielectric properties (ε′ and tan δ) of the core-shell nanoparticles, individual ε′ values of PTFE, PAAS, and PI were first measured and were found to be 2.1, 6.92, and 2.84, respectively. Note that the ε′ values of PAAS are much higher than that of PI due to the ionic nature of the salt. Therefore, it is expected that a higher ε′ value will be observed for PTFE/PASS core-shell nanoparticles than for PTFE/PI core-shell nanoparticles. As shown in Figure 6(A), the measured ε′ values of PTFE/PAAS core-shell nanoparticles are all higher than those of PTFE/PI core-shell nanoparticles confirming our expectation.

Figure 6(A) also shows that the measured ε′ values agree well with effective medium theory (EMT), which models how ε′ values change with composite composition. We previously reported on EMT and its applicability to core-shell architecture(s) when modeling dielectric properties.[35] The equation describing EMT is:

$$\varepsilon_{\text{eff}} = \varepsilon_m \left[1 + \frac{f(\varepsilon_f - \varepsilon_m)}{\varepsilon_m + n(1-f)(\varepsilon_f - \varepsilon_m)} \right] \quad (5)$$

Figure 6(A) shows that the increase of the PAAS and PI content in PTFE (5–35 wt %), increases ε′ values of both PTFE/PAAS core-shell nanoparticles (from 2.30 to 3.58) and PTFE/PI core-shell nanoparticles (from 2.14 to 2.38).

In addition to ε′, tan δ values for the core-shell nanoparticles were measured. It is noted in Figure 6(B) that different from ε′, the standard error of which is relatively low, the standard error for tan δ are quite high. One reason for the large tan δ standard error is due to the very small volume of sample. Such a small volume causes only a minute shift in the resonant frequency, therefore the Vector Network Analyzer must have a level of resolution to detect the shift. Nevertheless, the observed trend on tan δ values of PTFE/PI core-shell nanoparticles is similar to their ε′ values, showing an increasing trend with increasing PI content. Additionally, as expected, the tan δ

Table II. Results for Adhesion Testing in Accordance with ASTM F2252–03

Sample	Trial 1	Trial 2	Trial 3	Trial 4	Trial 5	Overall
100% PTFE	-	-	-	-	-	0/5
95% PTFE/5% PI	-	+	+	+	-	3/5
90% PTFE/10% PI	+	+	+	-	+	4/5
75% PTFE/25% PI	+	+	-	+	-	3/5
65% PTFE/35% PI	-	-	+	+	+	3/5

values of PTFE/PAAS core-shell nanoparticles are higher than those of PTFE/PI core-shell nanoparticles. Ultimately, the 5 wt % PI composite film provided the best dielectric properties out of the spray coated films in our study where $\varepsilon' = 2.14$ and $\tan \delta = 0.001$, which are suitable values for commercial applications.

CONCLUSIONS

A simple approach for preparing a low-k dielectric PTFE/PI core-shell nanoparticle by self-assembly of PTFE nanoparticles and PAAS through electrostatic interaction, followed by thermal imidization, is reported. The core-shell structure was characterized by FTIR and confirmed by TEM. SEM and AFM studies indicated that a porous material network with a smooth and continuous PI matrix on the surface, which helps to lower the ε' of the material. Besides excellent thermal stability with <0.4% weight loss at 500 °C, adhesion testing on the material showed good particle-to-particle and particle-to-substrate adhesion. Moreover, the dielectric properties measured at 7.2 GHz using cavity perturbation method were equally impressive, with a ε' of 2.14 and tan δ of 0.001 at 5 wt % PI. This represents the first reported PTFE/PI core-shell nanoparticle, which also provides a high performance, solution processable dielectric material for additive manufacturing.

ACKNOWLEDGMENTS

We gratefully acknowledge financial support from the NSF under CHE-1506209 for the purchase of chemicals and DMR-1533372 (YL).

NOMENCLATURE

f	volume fraction of filler (i.e. PTFE), dimensionless
f_c	resonant frequency of the original cavity (the substrate is in the cavity), Hz
f_s	resonant frequency of the perturbed cavity (the substrate with film is in the cavity), Hz
n	fitting factor, dimensionless
Q_c	quality factor of the original cavity, dimensionless
Q_s	quality factor of the perturbed cavity, dimensionless
Q'_c	theoretical quality factor, dimensionless
V_c	volume of the original cavity, m^3
V_s	volume of the film, m^3
tan δ	loss tangent, dimensionless
ε'	real part of the relative permittivity, dimensionless
ε''	imaginary part of the relative permittivity, dimensionless
ε_{eff}	ε' of the composite (i.e. core-shell nanoparticles), dimensionless
ε_f	ε' of the filler, dimensionless
ε_m	ε' of the matrix (i.e. PI), dimensionless

REFERENCES

1. Berman, B. *Business Horizons* **2012**, *55*, 155.
2. Kietzmann, J.; Pitt, L.; Berthon, P. *Business Horizons* **2015**, *58*, 209.
3. Hock, L. *RD Mag.* **2014**, *56*, 18.
4. Carlson, A.; Bowen, A. M.; Huang, Y. G.; Nuzzo, R. G.; Rogers, J. A. *Adv. Mater.* **2012**, *24*, 5284.
5. Lewis, G. K.; Schlienger, E. *Mater. Des.* **2000**, *21*, 417.
6. Gu, D. D.; Meiners, W.; Wissenbach, K.; Poprawe, R. *Int. Mater. Rev.* **2012**, *57*, 133.
7. Levy, G. N.; Schindel, R.; Kruth, J. P. *CIRP Ann. Manuf. Technol.* **2003**, *52*, 589.
8. Murphy, S. V.; Atala, A. *Nat. Biotechnol.* **2014**, *32*, 773.
9. Ochoa, I.; Hatzikiriakos, S. G. *Powder Technol.* **2005**, *153*, 108.
10. Scheirs, J. Polymer Recycling: Science, Technology, and Applications; Wiley: New York, **1998**.
11. Xiang, F.; Wang, H.; Yao, X. *J. Eur. Ceram. Soc.* **2006**, *26*, 1999.
12. Thomas, S.; Deepu, V. N.; Mohanan, P.; Sebastian, M. T. *J. Am. Ceram. Soc.* **2008**, *91*, 1971.
13. Thomas, S.; Raman, S.; Mohanan, P.; Sebastian, M. T. *Compos. A* **2010**, *41*, 1148.
14. Jin, S. Q.; Qiu, X.; Huang, B. Y.; Wang, L. X.; Zhang, Q. T.; Fu, Z. X. *J. Mater. Sci.* **2016**, *27*, 8378.
15. Jin, S. Q.; Wang, L. X.; Wang, Z. F.; Huang, B. Y.; Zhang, Q. T.; Fu, Z. X. *J. Mater.* **2015**, *26*, 7431.
16. Giani, E.; Sparnacci, K.; Laus, M.; Palamone, G.; Kapeliouchko, V.; Arcella, V. *Macromolecules* **2003**, *36*, 4360.
17. Antonioli, D.; Deregibus, S.; Panzarasa, G.; Sparnacci, K.; Laus, M.; Berti, L.; Frezza, L.; Gambini, M.; Boarino, L.; Enrico, E.; Comoretto, D. *Polym. Int.* **2012**, *61*, 1294.
18. Kapeliouchko, V.; Palamone, G.; Poggio, T.; Zuccheri, G.; Passeri, R.; Sparnacci, K.; Antonioli, D.; Deregibus, S.; Laus, M. *J. Polym. Sci. Part A: Polym. Chem.* **2009**, *47*, 2928.
19. Pozar, D. M. *IEEE Trans. Educ.* **1990**, *33*, 129.
20. O'Keefe, S.; Luscombe, C. K. *Polym. Int.* **2016**, *65*, 820.
21. Ghosh, M. K.; Mittal, K. L. Polyimides: Fundamentals and Applications; Marcel Dekker: New York, **1996**.
22. Misra, A. C.; Tesoro, G.; Hougham, G.; Pendharkar, S. M. *Polymer* **1992**, *33*, 1078.
23. Minges, M. L. ASMI Committee. Electronic Materials Handbook; ASM International: Materials Park, OH, **1989**.
24. Facinelli, J. V.; Gardner, S. L.; Dong, L.; Sensenich, C. L.; Davis, R. M.; Riffle, J. S. *Macromolecules* **1996**, *29*, 7342.
25. Birnbaum, G.; Franeau, J. *J. Appl. Phys.* **1949**, *20*, 817.
26. Sheen, J. *Measurement* **2005**, *37*, 123.
27. Zhou, H. R.; Yu, W. M.; Qu, C. Y.; Liu, C. W.; Wang, D. Z. *J. Mater. Sci.* **2015**, *26*, 9789.
28. Ramani, R.; Das, V.; Singh, A.; Ramachandran, R.; Amarendra, G.; Alam, S. *J. Phys. Chem. B* **2014**, *118*, 12282.
29. Nakamura, N.; Matsunaga, N.; Higashi, K.; Shimada, M.; Miyajima, H.; Yamada, M.; Enomoto, Y.; Hasegawa, T.; Shibata, H. Presented at the 2006 International Interconnect Technology Conference, 5–7 June 2006, Burlingame, CA, **2006**.
30. Uematsu, M.; Franck, E. U. *J. Phys. Chem. Ref. Data* **1980**, *9*, 1291.

31. Suwa, T.; Takehisa, M.; Machi, S. *J. Appl. Polym. Sci.* **1973**, *17*, 3253.
32. Kurabayashi, K.; Asheghi, M.; Touzelbaev, M.; Goodson, K. E. *J. Microelectromech. Syst.* **1999**, *8*, 180.
33. ASTM F2252/F2252M-13e1. Standard Practice for Evaluatig Ink or Coating Adhesion to Flexible Packaging Materials Using Tape. ASTM: West Conshohocken, PA, **2013**.
34. Ratta, V.; Stancik, E. J.; Ayambem, A.; Pavatareddy, H.; McGrath, J. E.; Wilkes, G. L. *Polymer* **1999**, *40*, 1889.
35. Poon, S. J.; Petersen, A. S. *Emerging Mater. Res.* **2012**, *1*, 286.